Revista Mexicana de Astronomía y Astrofísica, **41**, 147–154 (2005)

THE INTERACTION OF A JET-LIKE PULSE WITH A WIND FROM A STELLAR COMPANION

A. Riera,[1,2] A. C. Raga,[3] and J. Alcolea[4]

Received 2004 July 2; accepted 2005 February 17

RESUMEN

Presentamos simulaciones numéricas de la interacción entre un "pulso" bipolar colimado expulsado por una estrella y el viento continuo debido a una estrella compañera. Se muestra la variación de las propiedades de los mapas de intensidad en Hα al variar los valores de algunos de los parámetros de entrada. Mostramos que la asimetría (en el tamaño y la intensidad) entre los dos lóbulos de la nebulosa proto-planetaria OH 231.8+4.2 se puede explicar en el escenario propuesto si el viento de la estrella compañera muestra una fuerte dependencia con la latitud.

ABSTRACT

We present numerical simulations of the interaction between a collimated, bipolar "pulse" ejected from a star and a continuous wind ejected from a stellar companion. We explore the characteristics of the predicted Hα intensity maps by varying selected input parameters. We find that the asymmetry (in size and strength) between the two lobes of the proto-planetary nebula OH 231.8+4.2 is reproduced in this scenario if the wind ejected by the companion star has a strong latitude dependence.

Key Words: **ISM: KINEMATICS AND DYNAMICS — PLANETARY NEBULAE: INDIVIDUAL (OH231.8+4.2)**

1. INTRODUCTION

Most proto-planetary nebulae (PPNe) show bipolar or mutipolar lobes, highly collimated outflows or jets and other complex structures. A particularly well studied PPN candidate is the nebula associated with the OH 231.8+4.2 source. This is a remarkable example of a bipolar PPNe with collimated outflows. In Hα and forbidden emission line maps, this object presents a clear axial symmetry with the existence of shocked material in a wide, bipolar bubble with an obscuring ridge in between the two lobes (Bujarrabal et al. 2002). Long-slit spectra of this object show the presence of Herbig-Haro like knots at the end of the bipolar lobes, which probably trace the interaction between the fast, collimated molecular jet and the ambient material (Sánchez Contreras et al. 2000a). Contrary to what happens in most PPNe, the two optical lobes have different sizes; the Southern lobe is weaker but about two times more extended than the Northern lobe (Reipurth 1987; Sánchez Contreras et al. 2000a).

In the optical and NIR continuum, the nebula is narrow and elongated along its symmetry axis (Alcolea et al. 2001; Meakin et al. 2003). The same narrow component is observed in CO and other molecular emission lines (Alcolea et al. 2001; Sánchez Contreras, Bujarrabal, & Alcolea 1997; Sánchez Contreras et al. 2000b). The kinematical properties of this molecular jet are remarkable; its velocity increases linearly with distance from the star following a Hubble-like velocity law, which is consistent with a sudden acceleration event (Alcolea et al. 2001; Alcolea 2004). The Southern molecular jet (as seen in CO emission) is clearly more extended than the Northern jet and shows the highest flow velocity. The deprojected velocities show values of up to 430 km s^{-1} in the Southern jet, and up to 210 km s^{-1} in the Northern jet (Alcolea et al. 2001). The length along the axis of the OH 231.8+4.2 nebula is $\sim 50''$, which at a distance of 1.5 kpc (Kastner et al. 1992) implies a length $> 10^{18}$ cm.

[1]Departament de Física i Enginyeria Nuclear, Universitat Politècnica de Catalunya, Spain.
[2]Departament d'Astronomia i Meteorologia, Universitat de Barcelona, Spain.
[3]Instituto de Ciencias Nucleares, Universidad Nacional Autónoma de México, México.
[4]Observatorio Astronómico Nacional (OAN), Spain.

The central source of OH 231.8+4.2 is not detected at optical wavelengths because of the dusty envelope, but the reflected light has a M9 III spectral type, with a blue excess that suggests the presence of a warmer companion (or a peculiar photospheric structure and/or an accretion disk; Cohen 1981). This star is a typical Mira variable at the end of the asymptotic giant branch (AGB) identified with QX Pup (Kastner et al. 1998). Recently, OH 231.8+4.2 has been mapped at high spatial resolution in Si O and H_2O maser emission (Sánchez Contreras et al. 2002; Gómez & Rodríguez 2001). The position of the Si O and H_2O masers (which are tracing the position of QX Pup), is clearly offset from the axis of the bipolar outflow (as first pointed out by Gómez & Rodríguez 2001).

The QX Pup star shows the variability and maser emission properties typical of a Mira star (or of an OH/IR star) at the AGB. The contradiction between the apparent evolutionary stage of the nebula (i.e., PPN) and that of the QX Pup (AGB) star has been discussed by many authors (see, e.g., Alcolea et al. 2001). Based on the large displacement (> 1000 AU) between the position of the Si O maser and the bipolar axis of the nebula, Alcolea (2004) has proposed that QX Pup may not be directly related to the bipolar nebula. As first pointed out by Alcolea (2004), if the QX Pup star were located in the Northern lobe the observed differences between the two lobes could possibly be explained as a result of the interaction between the northern lobe and the wind from QX Pup.

In this paper, we present 3D numerical simulations of the interaction between a collimated, bipolar "pulse" ejected from a star and a continous wind ejected from a stellar companion. These simulations are a first attempt to reproduce the asymmetry between the two lobes of the bipolar PPN OH 238.1+4.2 in terms of a bipolar outflow/stellar wind interaction model. From the numerical simulations, we obtain predictions of Hα maps that can be compared with the optical images of OH 238.1+4.2 (Sánchez Contreras et al. 2000a; Bujarrabal et al. 2002).

The paper is organized as follows. In §2 we describe the parameters and the numerical method which have been used. In §3 we present the results of the numerical simulations. In §4 we compare our simulations with the observations of the PPN OH 231.8+4.2.

2. THE NUMERICAL MODELS

2.1. *General Considerations*

We compute a series of five models of the interaction between a collimated, bipolar "pulse" ejected from a star and a continuous wind ejected from a stellar companion. The models are computed in a 3D cartesian coordinate system, with its origin centered in the middle of the computational domain. The domain has a physical extent of 1.5×10^{18} cm along the z-axis, and of 7.5×10^{17} cm along the x- and y-axes. Outflow conditions are applied in all of the domain boundaries.

The computations are carried out with the "yguazú-a" code, which integrates the gasdynamic equations in a binary, adaptive computational grid. This code is described in detail by Raga, Navarro-González, & Villagrán-Muniz (2000). In the version of the code that we have employed, a single rate equation for neutral hydrogen is integrated (together with the 3D gasdynamic equations), and a simplified cooling function is calculated as a function of the density, ionization fraction and temperature (as described by Raga et al. 2000). This cooling function is then added as a sink term in the energy equation.

For our simulations, we have used a 5-level binary grid with a maximum resolution of 5.86×10^{15} cm along the three axes. The domain was initialized with a wind solution (§2.2) and a "bipolar pulse" (§2.3), and the simulations were carried out until the shell pushed out by the "pulse" reached one of the boundaries of the computational domain. The initial flow configuration is shown in Figure 1.

2.2. *The Wind*

We have initialized the computational domain with a wind with a latitude-dependent density of the parametrized form:

$$\rho = \frac{\dot{M}_w}{4\pi r^2}\, f(\theta)\,, \qquad (1)$$

where r is the spherical radius measured from the position of the wind source. The wind has an outward directed velocity (independent of r) given by:

$$v = \frac{v_w}{f(\theta)}\,, \qquad (2)$$

with $v_w = 40$ km s^{-1} for all of the computed models, and with different values of $\dot{M}_w$ for the successive models (see Table 1). The anisotropy function $f(\theta)$ has the parametrized form:

$$f(\theta) = \xi - (\xi - 1)\cos^p\theta\,, \qquad (3)$$

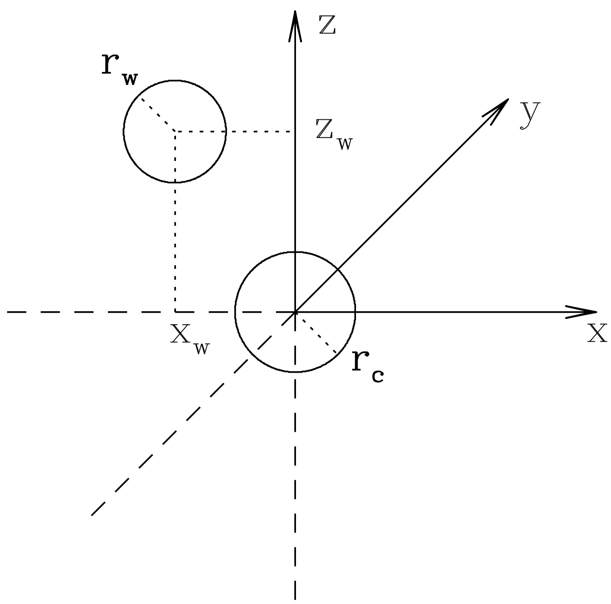

Fig. 1. Schematic diagram showing the configuration used for the numerical simulations (see the text). A collimated wind "pulse" is initialized within a sphere of radius r_c (centered at the origin of the coordinate system) and the continuous wind from the stellar companion is imposed (at all times) within a sphere of radius r_w, which is centered at the point $(x_w, 0, z_w)$. In the diagram, the projections of these two spheres on the xz-plane are shown. The axis of the "pulse" (as well as the axis of the wind in the simulations with a latitude-dependent wind) is parallel to the z-axis.

where θ is the angle measured from the polar axis of the wind (which we take to be parallel to the z-axis of the computational domain), ξ is a constant which is equal to the equator-to-pole density ratio, and p is a constant which determines the degree of flattening towards the equator of the density stratification. As can be seen from Eq. (3), a wind with $\xi = 1$ is isotropic. The choices of ξ and p for the computed models are given in Table 1.

The source of the wind is located at a position $(x_w, 0, z_w)$ away from the origin of the coordinate system (which is at the center of the computational domain, see Fig. 1 and §2.1). The values of x_w and z_w chosen for the computed models are given in Table 1. The whole of the computational domain (with the exception of the region occupied by the "bipolar pulse", see §2.3) is initialized with the wind solution, with the density and velocity given by Eqs. (1)-(3). Also, the wind solution is imposed at all times within a sphere of radius $r_w = 2.5 \times 10^{16}$ cm, centered on the $(x_w, 0, z_w)$ source position (see Fig. 1).

TABLE 1

COLLIMATED PULSE/WIND INTERACTION MODELS

Model	$\dot{M}_w$[a] $[10^{-6}\mathrm{M}_\odot\mathrm{yr}^{-1}]$	x_w[b] $[10^{17}\mathrm{cm}]$	z_w[b]	ξ[c]	p[c]	t_f[d] [yr]
M1	1	−1.0	1.5	1	—	1100
M2	5	−1.0	1.5	1	—	1500
M3	3	−1.0	1.5	20	0.5	1500
M4	10	−3.0	1.5	20	0.5	2300
M5	10	−3.0	1.5	50	0.5	2700

[a]Mass loss of the wind from the stellar companion.

[b]Position on the xz-plane of the stellar wind source.

[c]Asymmetry parameters of the wind.

[d]Time at which the expanding shell starts to leave the computational grid (the frames of Figs. 2–6 correspond to these times.)

We impose a uniform, $T_w = 10^3$ K within the sphere of radius r_w, and a temperature

$$T = T_w \left(\frac{r_w}{r}\right)^{2(\gamma-1)}, \tag{4}$$

outside of this sphere, where T_w and r_w are constants defined above, $\gamma = 5/3$ is the specific heat ratio and r is the spherical radius measured from the position of the wind source. This temperature stratification (corresponding to a constant velocity, adiabatic wind) is of course only used in the $r > r_w$ region as an initial condition. Finally, the ejected wind is assumed to have fully neutral H, and to have a small, seed ionization fraction coming from singly ionized C.

2.3. *The Bipolar Pulse*

As an initial condition, we impose a "bipolar pulse" of material ejected from a source located at the origin $(x, y, z) = (0, 0, 0)$ of the coordinate system (see Fig. 1). This bipolar "pulse" is imposed as an initial condition within a sphere of radius r_c (centered on the origin, see Fig. 1), and has a "hubble-like velocity law", a radially directed velocity of the form

$$v = v_c \left(\frac{R}{r_c}\right), \tag{5}$$

where R is the spherical radius (measured from the position of the bipolar outflow source), and a density

$$\rho = \rho_c \, g(\eta), \tag{6}$$

where

$$\eta = \frac{r_c \sin\theta_c}{R \sin\theta}, \tag{7}$$

and

$$g(\eta) = \min[1, \eta]\,. \tag{8}$$

Eqs. (6) to (8) give a cylindrically stratified density distribution, with a core of cylindrical radius $r_c \sin\theta_c$ of constant density ρ_c, and densities that fall monotonically for larger cylindrical radii. This kind of density stratification for the jet-like flow is inspired on the asymptotic MHD wind solution of Shu et al. (1995).

In all of our models we have considered $r_c = 5 \times 10^{16}$ cm, $n_c = \rho_c/(1.3 m_H) = 10^4$ cm^{-3} (where m_H is the mass of the hydrogen atom) for the central density of the "collimated pulse" [Eq. (6)], $\theta_c = 5°$ [Eq. (7)], and $v_c = 200$ km s^{-1}. For the "pulse" material (within the sphere of radius r_c, see above and Fig. 1) we have assumed a uniform temperature of 100 K, and that the gas is neutral (except for a seed ionization fraction coming from singly ionized C).

The bipolar "pulse" is then "released" at $t = 0$ (i.e., the material within the sphere of radius r_c is allowed to evolve freely as a function of time), and the gasdynamic equations are integrated in time to follow the interaction of the "pulse" with the stellar wind (described in §2.2). The results of the numerical integrations are described in the following section.

3. MODEL RESULTS

We have then computed 5 models (models M1–M5), with identical "bipolar pulses" (see §2.3) interacting with winds of different parameters (coming from the binary companion of the source of the bipolar pulse, see Fig. 1). We have tried both isotropic winds (models M1 and M2) and latitude dependent winds (models M3–M5, see Table 1), as described in §2.2.

In Figs. 2 to 6, we show some of the results obtained from models M1–M5 for the times t_f (see Table 1) at which the shell which is pushed out by the bipolar "pulse" reaches one of the boundaries of the computational domain. These figures show the density stratifications on the xz-plane (which includes the positions of both the wind and the "bipolar pulse" sources, see Fig. 1) and on the yz-plane. These Figures also show the Hα maps obtained by integrating the Hα emission coefficient (including the radiative recombination cascade and the $n = 1 \rightarrow 3$ collisional excitations) along the y- and x-axes.

The models with spherically symmetric winds (models M1 and M2, Table 1) produce highly asymmetric xz-plane density stratifications and xz-Hα emission maps (left hand side frames of Figure 2 and Figure 3). The upper lobe of the shell

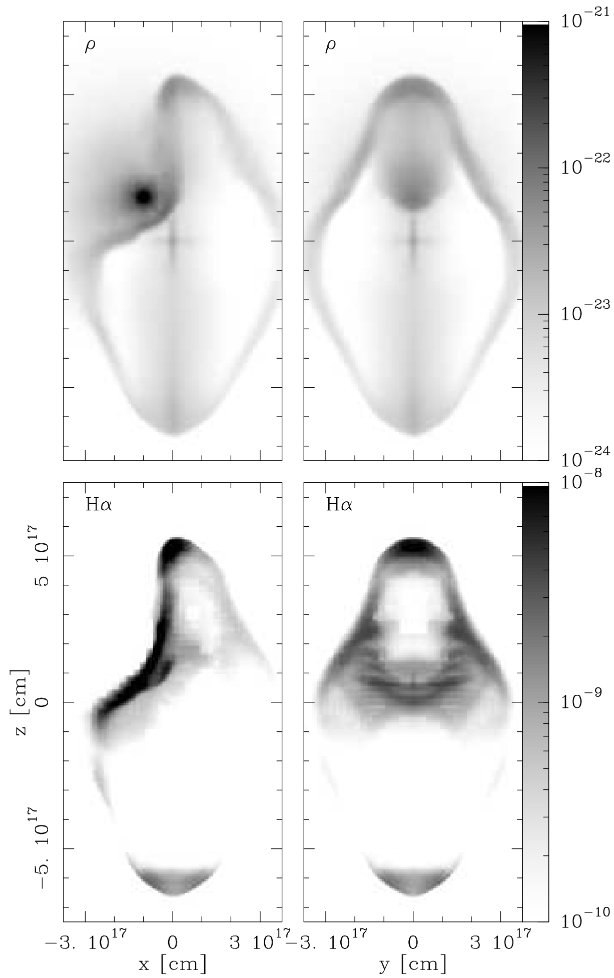

Fig. 2. Results obtained from model M1 for $t_f = 1100$ yr (see the text and table 1). The top frames show the density stratifications on the xz- (left) and yz-plane (right) with a logarithmic greyscale (given in g cm^{-3} by the bar on the right). The bottom frames show the Hα maps obtained by integrating the Hα emission coefficient along the y- (left) and x-axis (right) with a logarithmic greyscale (given in erg cm^{-2} s^{-1} sterad^{-1} by the bar on the right).

(which is pushed out by the bipolar pulse) shows a major "indentation" formed by the interaction with the dense region at the base of the stellar wind. The yz-plane cuts and Hα maps (right hand side frames of Figs. 2 and 3) show an upper lobe which is narrower and shorter than the bottom lobe, with a larger asymmetry for the model with larger mass loss rate (model M2, see Table 1).

In model M3, we have a wind mass loss rate intermediate between the ones of models M1 and M2 (see Table 1), but we have considered a

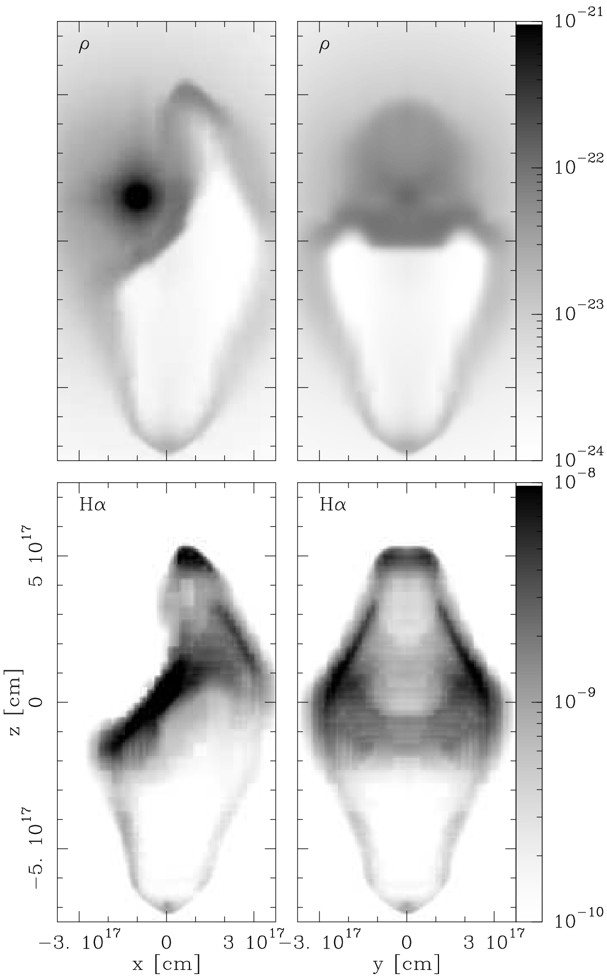

Fig. 3. Results obtained from model M2 for $t_f = 1500$ yr (see the text and Table 1). A description of the four frames is given in the caption of Fig. 1.

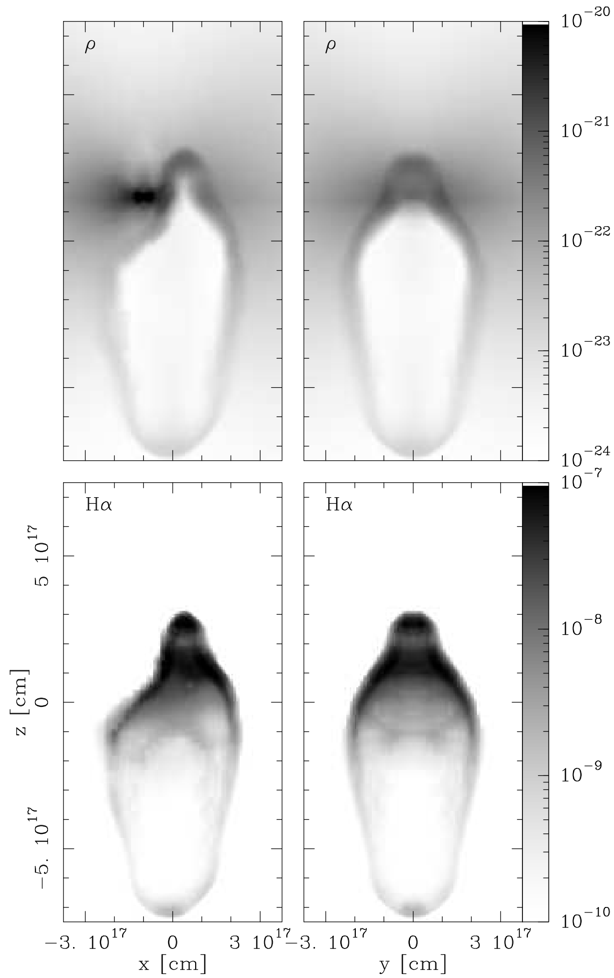

Fig. 4. Results obtained from model M3 for $t_f = 1500$ yr (see the text and Table 1). A description of the four frames is given in the caption of Fig. 1.

latitude-dependent wind (with $\xi = 20$ and $p = 0.5$, see Eq. [3]). In model M3 (see Figure 4), the bottom lobe of the outflow is somewhat narrower, but otherwise similar to the corresponding lobes of models M1 and M2 (see Figs. 2 and 3). The upper lobe of model M3, however, is strongly reduced in size, leading to a large asymmetry between the top and bottom lobes of the expanding shell.

In models M4 and M5 we have moved the stellar wind source away from the axis of the "bipolar pulse" ejection (see Table 1, and Figures 5 and 6). These models have a high mass loss rate, $\dot{M}_w = 10^{-5}\, M_\odot \mathrm{yr}^{-1}$, and two different degrees of asymmetry ($\xi = 20$ and 50 for models M4 and M5, respectively). These models produce top-to-bottom lobe asymmetries which are qualitatively similar to the ones obtained from model M3 (see above and Fig. 4).

As can be seen from the left hand side plots of Figs. 5 and 6, models M4 and M5 have the interesting property that the side-to-side asymmetries of the top lobe (when seen in the xz-plane density cut or Hα map) are much less important than the ones found in models M1–M3. This result indicates that a wind with a strong latitude dependence from a source placed well away from the axis of the "bipolar pulse" produces a strong asymmetry between the two lobes of the expanding shell, but does not introduce strong deviations from the initial axisymmetry of the bipolar pulse.

Models M4 and M5 show a double peak structure at the bottom lobe (see Figs. 5 and 6), which are reminiscent of the results obtained from numerical simulations of stellar jets for a high jet-to-environment density ratio (e.g., Raga 1988; Downes & Cabrit 2003).

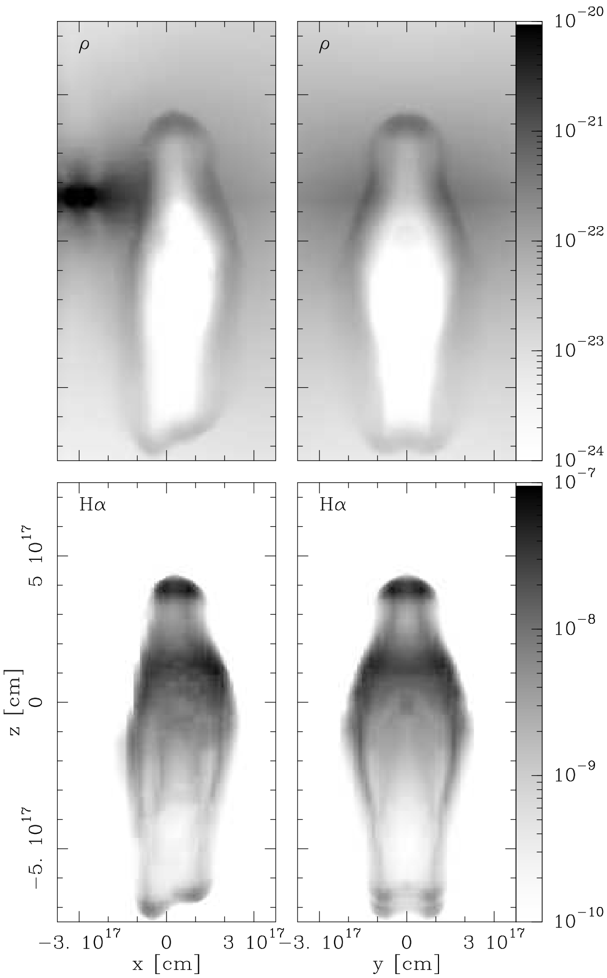

Fig. 5. Results obtained from model M4 for $t_f = 2300$ yr (see the text and Table 1). A description of the four frames is given in the caption of Fig. 1.

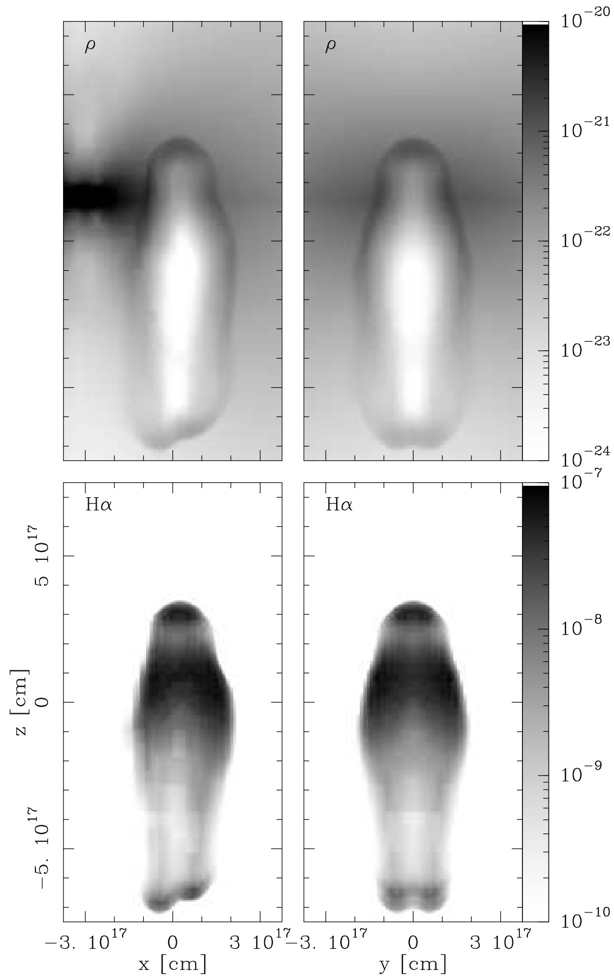

Fig. 6. Results obtained from model M5 for $t_f = 2700$ yr (see the text and Table 1). A description of the four frames is given in the caption of Fig. 1.

4. DISCUSSION

The results of our 3D numerical simulations of the interaction between a bipolar "pulse" and a continous wind ejected by a companion star indicate that the overall morphology (particularly, the strong differences between the sizes and velocities of the two lobes) of the PPN OH231.8+4.2 can be modeled as the result of such an interaction.

We have adopted a bipolar "pulse" (described by Eqs. [5] to [8]) instead of a continous jet, as an outflow of this kind appears to be implied by the observed Hubble-like velocity law (see §1). Also, we have taken the parameters (ρ_c, v_c, and θ_c), of the dense, high-velocity jet (see §2.3) that would be necessary for explaining the CO observations of OH 231.8+4.2 of Alcolea et al. (2001).

The parameters describing the wind from the companion star (i.e., QX Pup in the case of OH 231.8+4.2) are the wind velocity (v_w) and the mass loss rate ($\dot{M}_w$). We have adopted a value of 40 km s^{-1} for the wind velocity, which corresponds to the escape velocity from QX Pup (Alcolea 2004) and mass loss rate values characteristic of Mira variables (with values ranging from 10^{-6} to 10^{-5} $M_\odot$ yr^{-1}; see Table 1). We have considered a stellar wind with a latitude dependent density, with a density enhancement at the equator. The equator is perpendicular to the "bipolar pulse", as suggested by the spatial distribution of the SiO maser associated with QX Pup (Sánchez Contreras et al. 2002).

With these parameters we have computed several numerical simulations, from which we have obtained the Hα emission maps, that can be compared with the Hα images of OH 231.8+4.2 (Sánchez Contreras et al. 2000a; Bujarrabal et al. 2002).

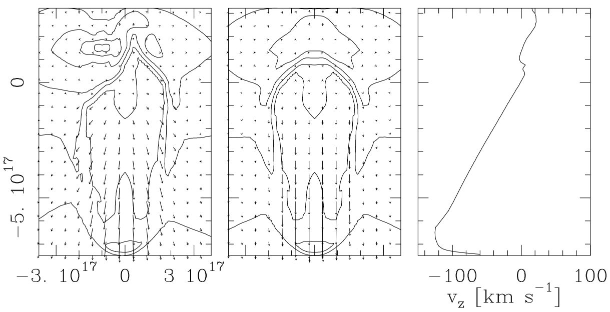

Fig. 7. Results obtained for model M3 for $t_f = 1500$ yr (see the text and table 1). The left and middle frames show the velocity field on the xz-plane (left) and yz-plane (middle). The velocity maps (arrows) are superposed on the density stratification, which is shown with linearly spaced isolines with steps of 5×10^{-22} g cm^{-3}. The right frame shows the axial velocity as a function of position along the symmetry axis of the bipolar pulse.

The numerical simulations reproduce qualitatively well several characteristics of the Hα image of OH 231.8+4.2. The observed and predicted Hα maps have bipolar structures with strong lobe-to-lobe asymmetries. We should point out that the hourglass morphology of OH 231.8+4.2 is not reproduced by these models. This discrepancy can be solved by including a dense disk (or torus) around the central source (as has been shown numerically by several authors; see, e.g., Frank & Mellema 1996). However, we have not included such a torus in the present simulations.

All of our models show an upper lobe which is narrower and shorter than the bottom lobe, but the large asymmetry between the Northern and Southern lobes of OH 231.8+4.2 is only reproduced by the models with a latitude dependent wind (M3–M5). Figs. 4, 5, and 6 illustrate that the upper lobe is strongly reduced in size in the latitude-dependent wind models, and that the ratio of ~ 2 between the sizes of the two lobes is in qualitative agreement with the observations of OH 231.8+4.2 (Bujarrabal et al. 2002). However, the width of the Southern lobe is better predicted by the models with spherically symmetric winds (models M1 and M2).

To illustrate the predicted velocity field, we present the velocity field of model M3 on the xz-plane and yz-plane (see Figure 7). For a comparison with the observed properties we also present the axial velocity along the symmetry axis (see Fig. 7). The predicted kinematics reproduces the strong velocity gradient observed along the nebular axis (Alcolea et al. 2001; Sánchez Contreras et al. 2000). However, we find that the model prediction gives velocities lower than the observed ones (by a factor of 3 to 4). In the top lobe, the model produces a too sharp drop in the velocity. In order to obtain a better agreement with the observations, we would need to have a model with a higher velocity bipolar pulse.

We have presented a number of 3D simulations of a bipolar pulse interacting with a continuous wind ejected by a close companion star. In our simulations, we have used a dense AGB wind with mass loss rates typical of AGB stars. We have shown that the strong asymmetries between both lobes of this nebula can indeed be explained in terms of a the proposed bipolar pulse/continuous wind interaction model (the companion star ejecting the wind has to be located within the Northern lobe). We find that the observed lobe-to-lobe asymmetry can be explained without invoking an intrinsic asymmetry in the ejection of the jet and the counterjet.

The work of ACR and was supported by the CONACyT grants 36572-E and 41320, and the DGAPA (UNAM) grant IN 112602. The work of ARi was supported by the Spanish MCyT grant AYA2002-00205. We acknowledge an anonymous referee for her/his helpful comments.

REFERENCES

Alcolea, J. 2004, in ASP Conf. Ser. Vo. 313, Asymmetric Planetary Nebulae III, eds. M. Meixner, J. Kastner, B. Balick, & N. Soker (San Francisco: ASP) 53
Alcolea, J., Bujarrabal, V., Sánchez Contreras, C., Neri, R., & Zweigle, J. 2001, A&A, 373, 932
Bujarrabal, V., Alcolea, J., Sánchez Contreras, C., & Sahai, R. 2002, A&A, 389, 271
Cohen, M. 1981, PASP, 93, 288
Downes, T. P., & Cabrit, S. 2003, A&A, 403, 135
Frank, A., & Mellema, G. 1996, ApJ, 472, 684
Gómez, Y., & Rodríguez, L. F. 2001, ApJ, 557, L109
Kastner, J. H., Weintraub, D. A., Zuckerman, B., Becklin, E. E., McLean, I., & Gatley, I. 1992, ApJ, 398, 552
Meakin, C. A., Bieging, J. H., Hora, J. L., & Tielens, A. G. G. M. 2003, ApJ, 585, 482
Raga, A.C . 1988, ApJ, 335, 820
Raga, A. C., Curiel, S., Rodríguez, L. F., & Cantó, J., 2000, A&A, 364, 763
Raga, A. C., Navarro-González, R., & Villagrán-Muniz, M. 2000, RevMexAA, 36, 67
Reipurth, B. 1987, Nature, 325, 787
Sánchez Contreras, C., Bujarrabal, V., & Alcolea, J. 1997, A&A, 327, 689
Sánchez Contreras, C., Bujarrabal, V., Miranda, L. F., & Fernández-Figueroa, M. J. 2000a, A&A, 355, 1103
Sánchez Contreras, C., Bujarrabal, V., Neri, R., & Alcolea, J. 2000b, A&A, 357, 651
Sánchez Contreras, C., Desmurs, J. F., Bujarrabal, V., Alcolea, J., & Colomer, F. 2002, A&A, 385, L1-L4
Shu, F. H., Najita, J., Ostriker, E. C., & Shang, H. 1995, ApJ, 455, L155

Javier Alcolea: Observatorio Astronómico Nacional, Apdo. 1143, E-28800 Alcalá de Henares, Spain. (j.alcolea@oan.es).

Alejandro C. Raga: Instituto de Ciencias Nucleares, UNAM, Apdo. Postal 70-543, 04510 México, D. F., México. (raga@nuclecu.unam.mx)

Angels Riera: Departament de Física i Enginyeria Nuclear, Universitat Politècnica de Catalunya, Av. Víctor Balaguer s/n, E-08800 Vilanova i la Geltrú, Spain. (angels.riera@upc.es).